



The Role of Immiscible Fingering on the Mechanism of Secondary and Tertiary Polymer Flooding of Viscous Oil

A. Beteta¹ · K. S. Sorbie¹ · K. McIver¹ · G. Johnson² · R. Gasimov² · W. van Zeil²

Received: 9 September 2021 / Accepted: 10 March 2022 / Published online: 5 April 2022
© The Author(s) 2022

Abstract

Immiscible viscous fingering in porous media occurs when a low viscosity fluid displaces a significantly more viscous, immiscible resident fluid; for example, the displacement of a higher viscosity oil with water (where $\mu_o > \mu_w$). Classically, this is a significant issue during oil recovery processes, where water is injected into the reservoir to provide pressure support and to drive the oil production. In moderate/heavy oil, this leads to the formation of strong water fingers, bypassed oil and high/early water production. Polymer flooding, where the injected water is viscosified through addition of high molecular weight polymers, has often been applied to reduce the viscosity contrast between the two immiscible fluids. In recent years, there has been significant development in the understanding of both the mechanism by which polymer flooding improves viscous oil recovery, as well as in the methodologies available to directly simulate such processes. One key advance in modelling the correct mechanism of polymer oil recovery in viscous oils has been the development of a method to accurately model the “simple” two-phase immiscible fingering (Sorbie in *Transp Porous Media* 135:331–359, 2020). This was achieved by first choosing the correct fractional flow and then deriving the maximum mobility relative permeability functions from this. It has been proposed that central to the polymer oil recovery is a fingering/viscous crossflow mechanism, and a summary of this is given in this paper. This work seeks to validate the proposed immiscible fingering/viscous crossflow mechanism experimentally for a moderately viscous oil ($\mu_o = 84$ mPa.s at 31 °C; $\mu_w = 0.81$ mPa.s; thus, $(\mu_o/\mu_w) \sim 104$) by performing a series of carefully monitored core floods. The results from these experiments are simulated directly to establish the potential of our modified simulation approach to capture the process (Sorbie, et al., 2020). Both secondary and tertiary polymer flooding experiments are presented and compared with the waterflood baselines, which have been established for each core system. The oil production, water cut and differential pressure are then matched directly using a commercial numerical reservoir simulator, but using our new “fractional flow” derived relative permeabilities. The use of polymer flooding, even when applied at a high water cut (80% after 0.5 PV of water injection), showed a significant impact on recovery; bringing the recovery significantly forward in time for both tertiary and secondary polymer injection modes—a further 13–16% OOIP. Each flood was then directly matched in the simulator with excellent agreement in all experimental cases. The simulations allowed a quantitative visualisation of the immiscible finger propagation from both water injection and the banking of connate water during polymer flooding. Evidence

of a strong oil bank forming in front of the tertiary polymer slug was also observed, in line with the proposed viscous crossflow mechanism. This work provides validation of both polymer flooding's viscous crossflow mechanism and the direct simulation methodology proposed by Sorbie et al. (Transp Porous Media 135:331–359, 2020). The experimental results show the significant potential for both secondary and tertiary polymer flooding in moderate/heavy oil reservoirs.

Keywords Viscous fingering · Immiscible displacement · Two-phase flow · Viscosity ratio · Viscous crossflow

Article Highlights

- **Observation of core scale viscous fingering at an adverse viscosity ratio of 1:100**
- **Proposed viscous crossflow mechanism during tertiary polymer flooding able to increase oil production by 40 % over waterflooding**
- **Viscous fingering experiments can be matched directly with a standard numerical reservoir simulator and a modified fractional flow approach**

1 Introduction

Immiscible viscous fingering has been studied since the 1950s (Engelberts and Klinkenberg 1951; van Meurs and van der Poel 1958) and is an important fluid instability phenomenon which occurs in a range of industries and applications (Homsy 1987). Here, we examine the role of immiscible viscous fingering during oil recovery processes, both in waterflooding and also in polymer flooding. During oil recovery, the initial pressure driven depletion (primary recovery) is often supplemented with water injection for pressure support and to aid sweep (secondary recovery). However, the *adverse viscosity ratio* (μ_o/μ_w) between the two fluids leads to poor displacement efficiency because of the fingering and low oil recoveries. We note that this is often expressed as “adverse mobility ratio”; we do not use this term here, although we do use the *local* strict definition of mobility ratio as follows:

$$M(S_w) = \left(\frac{\lambda_w}{\lambda_o} \right) = \left(\frac{k_{rw} \cdot \mu_o}{k_{ro} \cdot \mu_w} \right) \quad (1)$$

where λ , μ and k_r are mobility, viscosity and relative permeability, respectively, and the subscripts o and w refer to oil and water. The conventional meaning of “mobility ratio”, which we will denote M , is superficially similar to the above, but is defined as follows:

$$M = \left(\frac{k_{rw}(S_w=1 - S_{or}) \cdot \mu_o}{k_{ro}(S_w=S_{wi}) \cdot \mu_w} \right) \quad (2)$$

where the relative permeabilities for water and oil in M are evaluation at their *end points*, i.e. at $S_w=1 - S_{or}$ for k_{rw} and at $S_w=S_{wi}$ for k_{ro} . Another quantity that will be useful later is the total mobility, λ_T , which is given by:

$$\lambda_T = \lambda_W + \lambda_O = \left(\frac{k_{rw}}{\mu_w} \right) + \left(\frac{k_{ro}}{\mu_o} \right) \quad (3)$$

With the above concepts in mind, polymer flooding has been established as an effective method of improving oil recovery (Pye 1964; Sandiford 1964; Sorbie 1991) which works by increasing the aqueous phase viscosity of the injected water and hence reducing M (as defined above); but it is preferable to think of this increased water viscosity as reducing the (μ_o/μ_w) ratio. Viscosification of the aqueous injected phase is achieved by adding a relatively low concentration (C) of high molecular weight polymers, typically in the range $C \sim 300\text{--}2500$ mg/L.

Over the past few years, our understanding of the mechanisms which operate in polymer flooding has advanced quite significantly due to both the publication of high quality displacements experiments and some theoretical advances. This in turn has led to improved methods for optimising field polymer flood designs. Skauge et al. (2012) studied immiscible fingering in large sandstone slabs (30×30 cm) at very high mobility ratios $(\mu_o/\mu_w > 2000)$ using well-resolved X-ray scanning during the flooding processes. Strong water fingers were observed which were found to be sharpened and thinner at higher viscosity ratio. It was also observed that injection of tertiary polymer not only showed a sharp and significant increase in recovery, it also showed this response very quickly. Subsequent simulation and direct experimental observation has suggested that this was achieved by a viscous crossflow mechanism involving the flow of mobilised oil into the established water channels (fingers) (Skauge et al. 2012; Sorbie and Skauge 2019). Further work was performed by Skauge et al. (2014) where the same setup was used to examine waterflooding and polymer flooding of oils with viscosities between 5.1 and 616 mPa.s. Again, significant increases in recovery were observed for polymer flooding of the high viscosity oils (additional 35–40% OOIP). Intriguingly, the additional recovery by polymer flooding found for low viscosity oils was not only lower, but also pointed to the viscous crossflow mechanism requiring a certain viscosity ratio prior to taking effect. While water fingers were observed to form in 5.1 mPa.s and 66 mPa.s oils, they quickly collapsed into larger channels, trapping pockets of unswept oil. Furthermore, it was noted that an oil-polymer viscosity ratio of 30–60 was sufficient to achieve high recovery via tertiary polymer flooding and that increasing the polymer beyond that point would not result in higher recovery. For example, an oil of 2000 mPa.s may only require a polymer of viscosity $\sim 20\text{--}30$ mPa.s to significantly improve oil recovery. A similar finding was also found by Seright et al. (2018) in standard core plugs ($1.5'' \times 2\text{--}3''$) where the recovery of a 1600 mPa.s oil showed a large incremental response to polymer solutions up to ~ 20 mPa.s, and oil recovery was not further improved by polymer viscosities above 25 mPa.s.

Recent work has sought to explain these observations, applicable to many similar experiences by other authors such as the Pelican Lake polymer flood (Delamaide et al. 2014), through the concept of viscous crossflow. Sorbie and Skauge (2019) propose that polymer flooding cannot be fully ascribed to “mobility control” but that viscous crossflow is a major factor in many polymer flooding systems, beyond the “classic” layered system understanding such as that demonstrated by Sorbie (1991). In more viscous oil systems, the mechanism is described as the formation of initial water fingers which the polymer can then crossflow mobile oil into. As a result, 1D Buckley–Leverett theory (Buckley and Leverett 1942) cannot capture the intrinsically 2D/3D effects of polymer injection. While this may seem obvious to the reader, it is common practice for reservoir

engineers to obtain relative permeabilities/fractional flows through such analysis. Typically, oil displacement experiments have been analysed with JBN analysis (Johnson et al. 1959), based on Buckley–Leverett theory, or 1D numerical simulations (McPhee et al. 2015; Pereira et al. 2014) which inherently cannot capture fingering processes.

Sorbie et al. (2020) presented a robust method to obtain qualitative matches to the experimental results detailed previously. By starting with the correct fractional flow curves (denoted f_w^*) to describe the high saturations in the water fingers, the corresponding “maximum mobility” relative permeabilities are derived. When these derived functions were applied in a fine grid simulation using a random correlated permeability field, detailed finger patterns were observed showing qualitative matches to the observed experimental outputs, viz. immiscible finger patterns, recovery factors, water cuts and pressure drops. This method has recently been applied to the experiments performed by Skauge et al. (2014) with excellent agreement between the simulation and experiment for the time profiles of oil recovery, produced water fraction, pressure drop and the finger patterns (Salmo et al. 2022). The close agreement found between experimental results and simulation gives a clear indication that viscous crossflow is indeed the cause of these high recoveries. This work seeks to further validate the concept in relatively long cylindrical core plugs for a moderate oil viscosity ($\mu_o = 84$ mPa.s at 31 °C; $\mu_w = 0.81$ mPa.s). Both secondary and tertiary polymer flooding experiments are performed after performing a base line waterflood in all cases, and the experimental results are simulated directly using the new approach.

At this point, it should be noted that many authors have detailed methods for simulation of viscous fingering process, and a complete review is outside the scope of this publication; however, some recent work is discussed here. The reader is encouraged to refer to a comprehensive review that has been recently published by Pinilla et al. (2021). Broadly, methods can be characterised as either (1) numerical methods utilising high-resolution grids or (2) empirical methods designed to capture the average behaviour of the fingers (Juanes and Blunt 2006). Numerical methods can include computational fluid dynamics (CFD) utilising a Navier–Stokes (Clemens et al. 2013) or Lattice Boltzmann approaches (Dong et al. 2011); pore scale modelling (Lenormand et al. 1988; Regaieg et al. 2017); front tracking (Daripa et al. 1988); or high-resolution direct numerical simulation (Christie 1989). While computationally intensive, and thus not suitable for large models, these methods are highly capable of producing representative finger patterns and saturation changes. Tai and Muggerridge (2019) presented a comprehensive overview of common empirical models, Todd–Longstaff and Fayers, as implemented in reservoir simulation software (ECLIPSE-100) for miscible flooding. It was shown that such models were able to accurately predict the performance of miscible fingers but required significant calibration against field data and/or high-resolution simulations. Similarly, Luo et al. (2017) developed a fractional flow approach for empirically simulating immiscible displacement demonstrating the ability to achieve significantly improved experimental and field data matches vs. the “classical” methodology utilising JBN. It should be noted that among the myriad of simulation methodologies presented in the literature, the authors have found it relatively rare to see them evaluated directly against experimental observations.

The challenge emerges when moving to large field scale simulations where computational time is highly valuable. While reservoir simulators can be tuned using CFD or other numerical methods, this increases the complexity and resource requirements significantly when dealing with complex field scale simulations. The methodology proposed by Sorbie et al. (2020), and validated here directly against experiments, can be easily upscaled from the core plug to the field entirely within the reservoir simulator by simply applying the same relative permeability curves to both. This will be further demonstrated in

a forthcoming paper where the methodology and experimental data presented here are applied directly to an ongoing polymer flood in the North Sea.

2 Experimental and Modelling Methodology

2.1 Experimental

2.1.1 Polymer, Brine and Oil

The experiments carried out in this work use fluids and conditions relevant to a current polymer flood in an offshore oilfield (Field X). The polymer used in this work was an emulsion based, high molecular weight co-polymer of acrylic acid and acrylamide (HPAM). Dilution to the injection concentration was performed in two steps: first, the inversion of the emulsion to a 1% mother solution; and second, a dilution to the injection concentration (1800 mg/L). Both stages used impellor mixing at 500 rpm for 2 h and the same brine solution was used throughout, Table 1. Flow curves (viscosity vs. shear rate) for 500–3500 mg/L polymer solutions at reservoir temperature ($T=31\text{ }^{\circ}\text{C}$) are shown in Fig. 1. The 1800 mg/L polymer solution has a lower Newtonian viscosity plateau of, $\mu_p=22\text{ mPa.s}$.

A dead crude oil sample from Field X was used as the oil phase. In order to match the live oil viscosity ($\mu_o=84\text{ mPa.s}$) at reservoir temperature ($T=31\text{ }^{\circ}\text{C}$), the oil was diluted with a light mineral oil.

The rheology of the injected fluids was measured using an Anton Paar MCR302 with double gap geometry (DG42-XL). A summary of the fluid viscosities is presented in Table 2.

2.1.2 Core Flooding

Bentheimer (a quartz-rich, highly permeable and relatively homogenous sandstone) cores were sourced from Kocurek Industries. Longer cores (of diameter, $D=3.81\text{ cm}$ and length, $L=25.4\text{ cm}$) were used in order to reduce capillary end effects and to reduce the error in oil recoveries measured volumetrically. At key stages of all floods, the overall volumetric recoveries were checked using tracer floods, which give a very accurate estimate of these quantities (Shields et al. 2006). The absolute permeability to brine and porosity of each core is given in Table 3. From here on, polymer flooding from S_{wi} will be referred to as secondary polymer flooding, while polymer flooding after a period of waterflooding will

Table 1 Field X Brine Composition

Ion	mg/L
Na	5048
Ca	569
Mg	210
Cl	9404
TDS	15,231

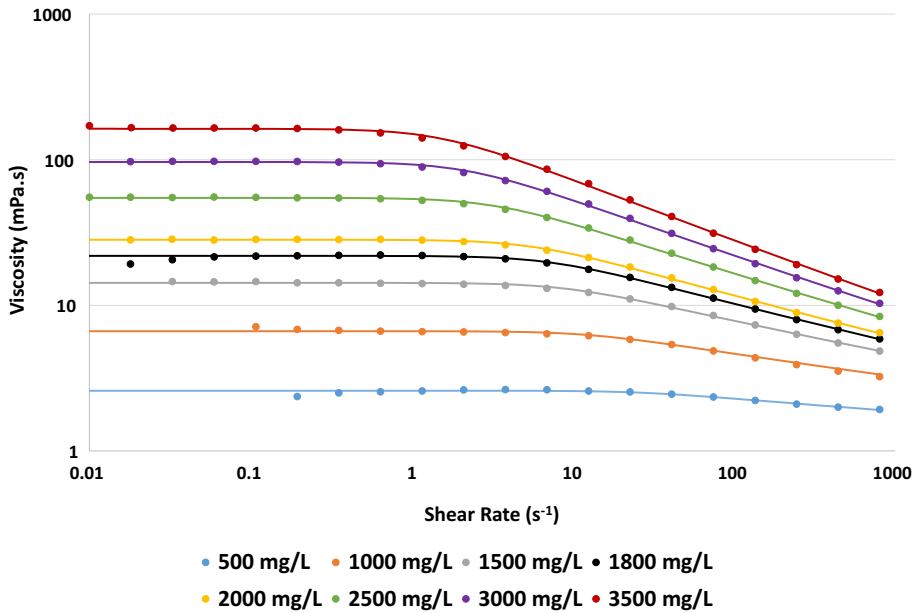


Fig. 1 Polymer Flow Curves at Reservoir Temperature (31 °C)

Table 2 Injection Fluid Viscosities

Fluid	Viscosity (mPa.s) ± 2%
Brine	0.81
1800 mg/L Polymer (Newtonian Plateau)	22.2
Light Mineral Oil	1.02
Heavy Mineral Oil	88
Dead Crude Oil (Viscosity Matched to Live Oil)	84

Table 3 Core Properties for each of the flooding cycles CF1, CF2 and CF3

Code	Flood	Absolute Permeability to Brine (D)	Porosity (%)
CF1	Secondary Polymer	2.8 ± 0.2	24.8 ± 0.3
CF2	Tertiary Polymer 1	2.5 ± 0.2	25.7 ± 0.3
CF3	Tertiary Polymer 2	2.1 ± 0.2	25.0 ± 0.3

be denoted tertiary polymer flooding. Three flooding cycles, denoted CF1–CF3, were carried out as labelled in Table 3 and described as follows:

- *CF1* Core 1—a waterflood from $S_w = S_{wi}$, core reconditioning to initial water saturation, S_{wi} , then a *secondary* polymer flood ($\mu_p = 22$ mPa.s) immediately from S_{wi} ;
- *CF2* Core 2—a waterflood from $S_w = S_{wi}$, reconditioning to S_{wi} , then a waterflood for 0.5 PV (where water cut ~ 80%) then a *tertiary* polymer ($\mu_p = 22$ mPa.s) flood;

- *CF3 Core 3*—a waterflood, reconditioning to S_{wi} , then a waterflood for 0.5 PV (where water cut $\sim 80\%$) then a reduced viscosity *tertiary* polymer ($\mu_p = 11$ mPa.s) flood.

Cores were inserted into Viton sleeves then mounted vertically in a bi-axial core holder with an overburden pressure of 500 psi. Injection was performed from bottom to top, either directly from a Strata DCP-50 pump or, in the case of crude oil, via a piston vessel mounted inside the core flood rig. For each polymer flood, a “baseline” waterflood was first performed to establish a benchmark for each specific core to remove any ambiguity when assessing the effect of the polymer. The core was then re-saturated with oil back to the same initial water saturation (S_{wi}) prior to performing the polymer recovery experiments. The initial conditions ($S_w = S_{wi}$) were accurately established for all cores (see below). A description of the main stages in the injection cycle for each flood is given in Table 4. It should be noted that the first 12 steps are identical between each of the 3 cores.

Light mineral oil was used when establishing S_{wi} to allow the use of in-line UV tracers to measure pore volume to water; when dosed with 10 mg/L trans-stilbene, the light mineral oil shows a strong UV absorbance at 316 nm (Shields et al. 2006). A similar in-line tracer process was used during aqueous characterisation, using 10 mg/L NaI in the brine phase and using UV detection at 230 nm (Shields et al. 2006). Permeability is calculated from Darcy’s law by measuring the pressure drop at five flow rates and calculating the permeability from the slope of the flow rate/pressure drop plot, for that saturation stage.

Polymer retention was measured by comparing the breakthrough curve to that of a co-injected lithium tracer as shown in Eq. 4.

$$\Gamma = \left(\Sigma \Delta PV \cdot \frac{C_{Tracer}}{C_{Tracer_0}} - \Sigma \Delta PV \cdot \frac{C_{Polymer}}{C_{Polymer_0}} \right) \cdot C_{Polymer_0} \cdot \frac{PV}{M_{Rock}} \quad (4)$$

Table 4 Core Injection Sequence

Step	Secondary Polymer	Tertiary Polymer	Saturation Determination
1	100% Water Saturation		In-line UV—NaI
2	Light Mineral Oil to S_{wi}		In-line UV—trans-stilbene
3	Heavy Mineral Oil to Lower S_{wi}		Measured at next stage
4	Light Mineral Oil at S_{wi}		In-line UV—trans-stilbene
5	Crude Oil		No saturation change
6	Crude Oil Aged for 14 days		No saturation change
7	Waterflood		In-line UV—NaI
8	Bump Waterflood		In-line UV—NaI
9	Light Mineral Oil to S_{wi}		In-line UV—trans-stilbene
10	Heavy Mineral Oil to Lower S_{wi}		Measured at next stage
11	Light Mineral Oil at S_{wi}		In-line UV—trans-stilbene
12	Crude Oil		No saturation change
13	–	0.5 PV Waterflood	Volumetric
14	Polymer Flood	Polymer Flood	Volumetric
15	Water Flush	Water Flush	In-line UV—NaI

where C_{Tracer} is the concentration of tracer in the effluent, $C_{Tracer0}$ is the concentration of injected tracer, $C_{polymer}$ is the assayed polymer concentration, $C_{polymer0}$ is the injected polymer concentration, PV is the volume of one pore volume, ΔPV is the change in injected pore volume and M_{Rock} is the mass of the core. Polymer concentration was determined using the Hyamine method (Beteta et al. 2021) while the lithium tracer concentration was measured using inductively coupled plasma optical emission spectroscopy (ICP-OES). A polymer concentration of ~0.5 mg/L is considered to be the minimum detectable polymer concentration using the Hyamine method, and this is therefore taken as being the complete polymer return (although some polymer is irreversibly retained in the core).

All recovery stages were performed with a constant injection velocity of, $v=(Q/(A.\phi))=3.05$ m/day (i.e. $Q=36$ ml/hour for the laboratory pumps); where Q is the volumetric injection rate, A is core cross-section and ϕ is the porosity. A moderate/high injection rate compared to typical reservoir advancement rates has been used to minimise the effect of gravity and to overcome any capillary end effects. This frontal advance rate is in fact quite comparable with the reservoir field flow rates that this study relates to.

2.2 Simulations

The core flood experiments were modelled using CMG STARS and a 2D representation of the core plugs using the method developed by Sorbie et al. (2020). Using this approach, the quantification of viscous fingering processes in porous media can be broken down into 3 key requirements:

1. Tuning the relative permeability (RP) curves to give the desired fractional flow curve, f_w^* . It is this fractional flow that is essentially the main “input”, and the RP curves are further adjusted until the maximum mobility, λ_T , is achieved while still honouring this “input f_w^* ”;
2. Using a heterogeneous permeability field with an appropriate permeability range and correlation length, since any porous media system will be heterogeneous at the small scale. In fact, a correlated random field (CRF) is used with a given correlation length and level of heterogeneity described by the Dykstra-Parson coefficient (V_{DP}) (Dykstra and Parsons 1950);
3. Using a sufficiently fine grid such that correlation length is significantly larger than the grid cell size.

Step 1 above is the essential core of the method, and a full description of the simulation approach, described briefly above, is given in Sorbie et al (2020).

In order to have greater control over the form of the corresponding fractional flow curve, additional constants have been added to the analytical forms of the relative permeability curves as shown in Eq. 5.

$$k_{rw}(S_w) = \frac{\alpha_w}{\left[1 + \beta_w \left(\frac{S_{wn}}{S_{on}}\right)^{-\gamma_w}\right]^{1/\delta_w}} \text{ and } k_{ro}(S_w) = \frac{\alpha_o}{\left[1 + \beta_o \left(\frac{S_{on}}{S_{wn}}\right)^{-\gamma_o}\right]^{1/\delta_o}} \tag{5}$$

where S_{wn} and S_{on} are the normalised water and oil saturation, respectively; $S_{on} = 1 - S_{wn}$ and $S_{wn} = \frac{S_w - S_{wi}}{(1 - S_{or} - S_{wi})}$; α_w , α_o , δ_w , and δ_o are the normal Brooks-Corey parameters; and β_w , β_o , γ_w , and γ_o are the additional constants used to tune the fractional flow curve.

The form of the relative permeabilities requires 8 parameters, where 4 of them are the normal Corey parameters and the other 4 have a different purpose. However, the form of the relative permeabilities is not really of concern here; it is the form of the fractional flow (f_w^*) that is of primary concern (which establishes a ratio of relative permeabilities), and that we use assumption of a maximum mobility to close the equations. When this is done, then we have the required relative permeabilities for the method as per the study from Sorbie et al. (2020). Indeed, the relative permeabilities here are relegated to the role of “pseudo functions” which match all aspects of the data; viz. recoveries, water cuts, pressure drops and additional predicted incremental recovery by polymer.

It should be noted that the simulations presented here and in Sorbie et al. (2020) do not include capillary pressure (P_c), since it is known that the system is viscous dominated. The expression for the capillary length scale is given in this previous publication and our assumption is that the numerical dispersion of the grid includes this effect. Capillary pressure can stabilise immiscible fingers (Yortsos and Hickernell 1989) at sufficiently short length scales (Berg and Ott 2012; Jerauld et al. 1984). However, a conflict arises when this understanding is compared to visualised immiscible displacement experiments. For example, in the floods performed by Skauge et al. (2014) at a range of viscosity contrasts in Bentheimer slabs, very distinct fingers are clearly observed which form within less than ~ 1 cm. A full discussion is outside the scope of this publication; however, both the magnitude and form of the capillary pressure curve are critical for direct simulation of viscous fingers—this will be demonstrated in a forthcoming publication.

The base case simulation model of the experimental core is defined by 100×100 cells with a random correlated permeability field generated through a lognormal distribution using a correlation length of one tenth of the core diameter and a Dykstra–Parsons coefficient of, $V_{DP} = 0.66$. Porosity is set to be constant throughout the core (ϕ as in Table 3 for that flooding cycle), and the resulting permeability field is shown in Fig. 2. A sensitivity study to both correlation length and permeability contrast was performed alongside the presented simulations. As expected, the presence of larger heterogeneities, i.e. a high dimensionless correlation length, leads to the formation of fewer but larger fingers. However, only minor variation was observed in the recovery, water cut and pressure drop under the studied conditions. A larger sensitivity to correlation length was reported by Salmo et al. (2022) and Sorbie et al. (2020) for a significantly higher viscosity contrast ($\mu_o/\mu_w > 1600$).

The same permeability field is used for all simulated core plugs, with the actual permeability values scaled to match the average permeability measured in the experiment.

In the examples presented here, the polymer solution is treated as a Newtonian fluid (i.e. not shear thinning/thickening)—a set of assumed *in situ* rheology curves were examined using the Newtonian viscosity as a starting point and no impact was observed in the recovery/water

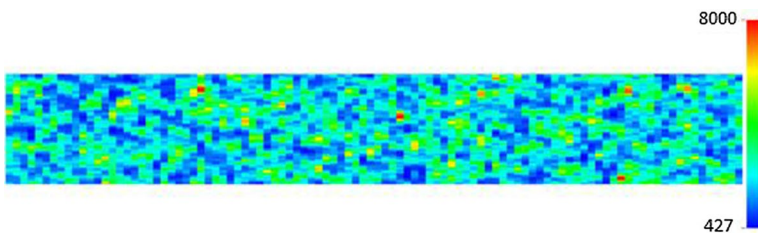


Fig. 2 Random Correlated Permeability Field Used in Simulations—Actual Values of Each Cell Scaled to Average Permeability of Specific Core Plug

cut profiles. However, it should be kept in mind that the apparent viscosity in the porous media may be higher/lower than the Newtonian value—although, as demonstrated below, the system presented here was not found to be overly sensitive to the viscosity of the polymer solution.

3 Results

3.1 Establishing a Waterflood Baseline

In order to ensure a fair and accurate assessment of the recovery from each of the polymer floods under secondary and tertiary conditions, a baseline was established in each core for the corresponding waterfloods. The outcrop Bentheimer cores were first saturated with Field X injection brine and characterised, for permeability and porosity/pore volume. Following this, a light mineral oil was injected to de-saturate the core to S_{wi} and the core characterisation was repeated. The initial S_{wi} obtained at this stage, $> 20\%$, was felt to be unrepresentative of field conditions ($S_{wi} \sim 9\%$), and therefore, a heavy mineral oil (viscosity matched to field crude) was injected to drive the S_{wi} down further ($S_{wi} \sim 14\%$). The core was then re-saturated (miscibly) with the light mineral oil to repeat the characterisation steps. The core was then saturated with dead crude and the permeability re-measured. After crude saturation, the core was aged at reservoir temperature ($T=31\text{ }^{\circ}\text{C}$) for 14 days to condition the wettability towards a more oil-wet system. Upon completion of the ageing process, the permeability to oil was re-measured and found to be in good agreement with the original measurement in all cases. The core properties prior to waterflooding are shown in Table 5.

Thus, an appropriate S_{wi} was established and a well-characterised baseline waterflood was performed for each separate core, prior to the polymer injection. Water was injected at a constant rate to give a frontal velocity of $v \sim 3\text{ m/day}$ ($Q=36\text{ ml/hour}$), with effluent samples collected for analysis in 0.03 PV increments (2 ml). The oil production vs. time in PV is measured volumetrically and final total recovery was confirmed by tracer measurements at the end of the injection period.

Excellent agreement was observed between the three baseline waterfloods for CF1, CF2 and CF3, as shown in Fig. 3 and Table 6, where the minor differences seen between them are entirely within acceptable limits of core-to-core variation. Thus, a comparison can be made both between waterflooding and polymer flooding, as well as between the mode (secondary vs. tertiary polymer injection) of recovery and the impact of polymer viscosity on tertiary flooding (the latter was studied in CF3).

The differential pressure profile shows classic two-phase displacement behaviour for a viscous oil; as the high viscosity oil is driven from the core, a sharp continuous reduction in pressure drop across the core over the first ~ 0.3 PV of water injection is observed. This sharp pressure drop is a strong indicator that immiscible viscous fingering is occurring in these waterfloods. Here, it is useful to refer to the M-paradox discussed by where it is noted that the early water breakthrough and sharp drop in pressure

Table 5 Core Properties Prior to Waterflood: CF1—Secondary Polymer Flood; CF2—Tertiary Polymer Flood; CF3—Reduced Viscosity Tertiary Polymer Flood

Core	CF1	CF2	CF3
S_{wi} (%)	14 ± 0.3	13 ± 0.3	16 ± 0.3
Permeability to Oil (D)	2.6 ± 0.2	2.1 ± 0.2	2.1 ± 0.2

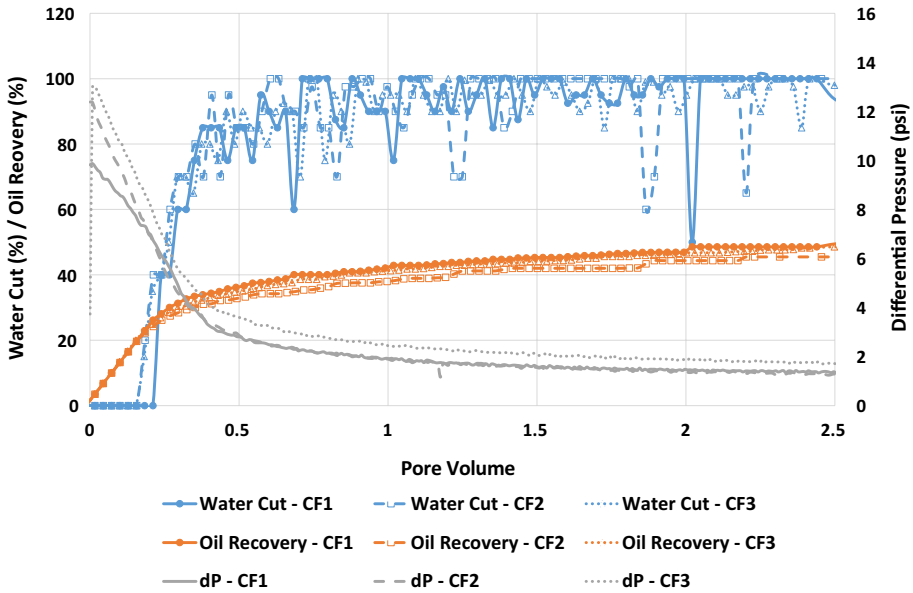


Fig. 3 Recovery Profile for Baseline Waterfloods: CF1—Secondary Polymer Flood; CF2—Tertiary Polymer Flood; CF3—Reduced Viscosity Tertiary Polymer Flood. Baseline Water Performance Established through Excellent Repeatability Observed Between Each Flood

Table 6 Core properties post waterflood

Core	CF1	CF2	CF3
Oil Recovery (%)	49 ± 2	46 ± 2	49 ± 2
Oil Saturation (%)	44 ± 2	47 ± 2	41 ± 2
Permeability to Water (mD)	269 ± 27	265 ± 27	264 ± 26

could be due to low oil mobility and low water saturation in the fingers. However, this is not consistent with all of the experimental observations of *in situ* unstable immiscible displacement, e.g. Skauge et al. (2014); van Meurs and van der Poel (1958), where high water saturation in the fingers is observed. Thus, a methodology based on achieving the correct fractional flow is a requirement for simulation of immiscible fingers.

In terms of displacement efficiency, it can be seen that the water breaks through at 0.15 PV—0.2 PV, which is also a very clear marker of viscous fingering. Following breakthrough, the water cut rises to ~80% after 0.4 PV then more gradually reaches an approximate plateau at ~1.5 PV. Following this, there is sporadic release of oil for the remainder of the flood. This water production should in theory be more continuous but there can be “hold up” in the system, and so it is the averaged behaviour that is more important. Oil production, of course, follows the inverse of this behaviour with the recovery, % original oil in place (OOIP), reaching 22–25% by the time of water breakthrough.

In all three cases, a high rate “bump” waterflood (~25.6 m/day–300 ml/hr) was performed following the measurement of permeability and pore volume, although no further oil was mobilised.

Table 7 Core properties prior to polymer injection

Core	CF1	CF2	CF3
S_{wi} (%)	14 ± 0.3	15 ± 0.3	14 ± 0.3
Permeability to Oil (D)	2.8 ± 0.2	2.1 ± 0.2	1.9 ± 0.2

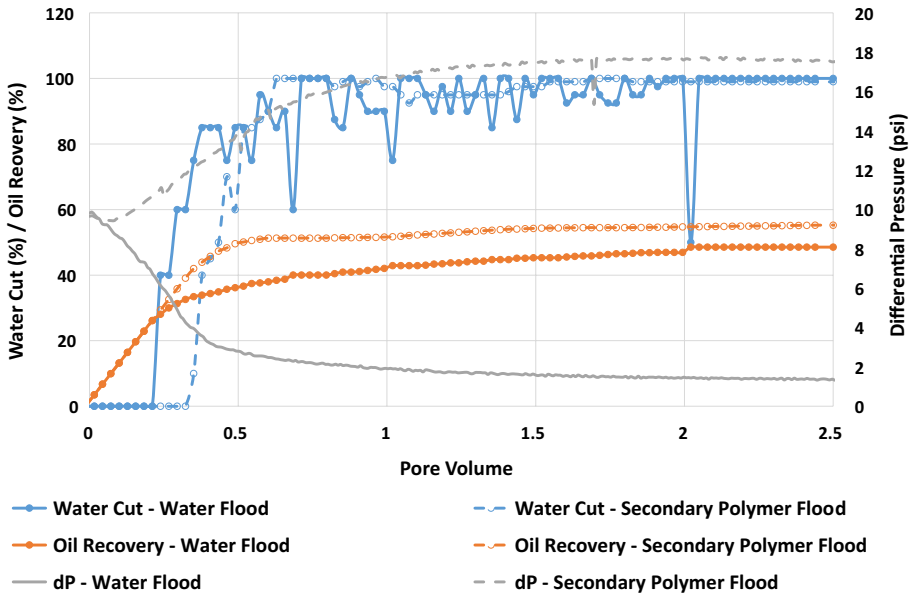


Fig. 4 Secondary Polymer Flooding versus Waterflooding for CF1 Flooding Cycle. Application of Polymer Flooding in Secondary Mode Brings Recovery Significantly Forward in Time versus Waterflooding

With baseline performance for waterflooding established, the cores were reconditioned back to S_{wi} —reaching values in excellent agreement with both the previous saturation (S_{wi}) as well as each other as shown in Table 7.

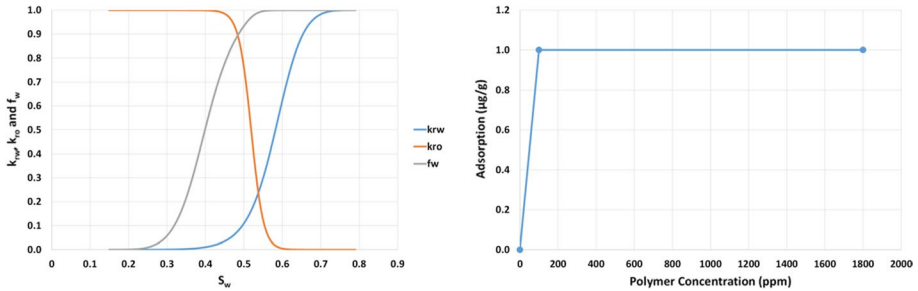
3.2 Secondary Polymer Flood

With the waterflood baseline and representative S_{wi} established, an 1800 mg/L polymer solution was immediately injected into the core (CF1) at 3 m/day; i.e. this is a secondary polymer flood. The production and pressure profile are shown against the baseline waterflood in Fig. 4.

The potential for secondary polymer flooding is immediately clear, by replacing water injection with viscous polymer water breakthrough is delayed from 0.21 to 0.32 PV with a corresponding increase in recovery of 13.4% OOIP by 0.5 PV of injection. As further volumes are injected, the difference between recoveries decreases to 9.5% OOIP at 1.0 PV, 8.93% OOIP at 1.5 PV and 6.7% OOIP at the end of the flood (2.5 PV). In other words, the application of the secondary polymer “brings forward” the oil production in “time” (PV injected), which is the classical mechanism in polymer flooding (Sorbie 1991).

Table 8 Secondary polymer flood relative permeability coefficients, adsorption and RRF

α_w	1.0	β_w	17.00	γ_w	4.0	δ_w	1.0	Γ	1 $\mu\text{g/g}$
α_o	1.0	β_o	0.05	γ_o	10.0	δ_o	1.0	RRF	5.5

**Fig. 5** Secondary Polymer Flood Relative Permeability, Fractional Flow (left) and Adsorption Isotherm (right)

Minimal polymer adsorption was measured in the core. We note that there may be some effect of IPV (inaccessible pore volume) which slightly masks the effect of adsorption, but the adsorption level is very low and would be barely observable for the input polymer concentration used here (1800 mg/L). Following the polymer injection, the core was flushed with brine at ~ 3 m/day for > 50 PV until the effluent showed < 0.5 mg/L polymer concentration using the Hyamine method. At this point, the permeability to water was determined and the residual resistance factor, RRF, was determined (see Sorbie 1991). Relative to the permeability measured after the waterflood, the RRF was ~ 3.1 , but it may be even higher than this value due to the difference in saturation between the original waterflood and polymer flood.

Direct simulations of all the core floods reported in this paper (water and polymer floods) were carried out using the fractional flow approach for simulating unstable immiscible displacements given by Sorbie et al. (2020) and described briefly above. In this approach, observation of the required (relatively high) water saturation in the immiscible fingers guides our choice of fractional flow. The relative permeabilities are then derived by aiming to maximise the total mobility, $\lambda_T(S_w)$ (see Eq. 3), for the experimental oil and water viscosities ($\mu_w = 0.81$ mPa.s; $\mu_o = 88$ mPa.s), while honouring the chosen fractional flow, f_w^* . The fractional flow is then adjusted until a successful match was observed between experiment and simulation for the waterflood; the same derived relative permeability functions are then used without any further adjustment to forward predict the polymer flood in either secondary or tertiary mode. The final inputs from this procedure, which is described in detail in Sorbie et al (2020), are given in Table 8 and Fig. 5.

The secondary polymer flood showed a lower than measurable level of polymer adsorption although this did cause a measured $\text{RRF} = 5.5$; to match this, we assumed a very low nominal polymer adsorption level of 1 mg/g as shown in Fig. 5 (on right), which then triggered an $\text{RRF} = 5.5$ at full adsorption.

The experimental versus simulation match for the baseline waterflood and the secondary polymer flood are given in Figs. 6 and 7, respectively.

Both waterflooding and secondary polymer flooding are well matched with this method. There is some variance in the magnitude of the simulated pressure response; however, the shape of the profile is very close to that observed in the experiments. As the relative permeabilities are non-unique, it is possible that further alteration may bring the simulated pressure response further into line with the experiment.

No in situ imaging, such as computerized tomography scanning, was available for the core floods reported here. However, we will treat the matched simulations as our “numerical visualisation” of the various floods. Both the waterflood and secondary polymer flood “visualisations” from the simulation clearly indicate the formation of distinct viscous fingers, as shown in Fig. 8. The viscous fingering is most evident for the baseline waterflood, but the instability does not vanish entirely for the secondary polymer flood.

It can be seen that the addition of polymer to the injected fluid stabilised the flood front to some degree. However, water fingers do still form during the secondary polymer flood which arise due to the connate water in the core being banked ahead of the polymer slug, which then fingers into the viscous oil. This effect is illustrated more clearly in Fig. 9 where the water saturation and polymer concentration are shown during polymer propagation in the secondary polymer flood. Note that the polymer concentration (red) shows a stabilised front but the viscosity of the fluid in the fingers is the same as the water viscosity (blue).

The interpretation and significance of the secondary polymer flood become more evident given the results of the tertiary polymer flood; i.e. when polymer injection after 0.5 PV of water injection, when the water cut is 80%. Results from the tertiary polymer flood are presented in the following section.

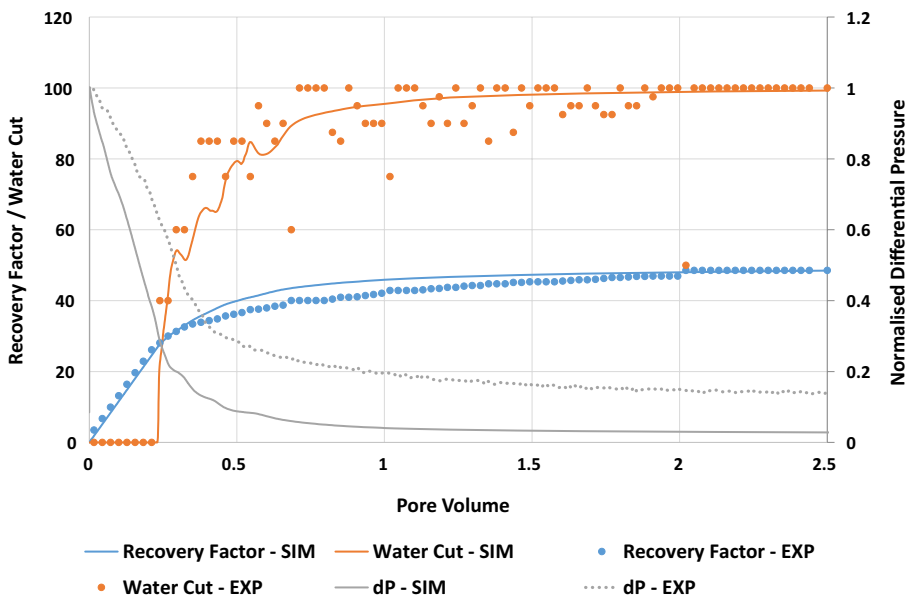


Fig. 6 Secondary Polymer Flood—Waterflood Baseline for CF1—Experiment versus Simulation Match. Oil and Water Production is Well Matched. The Shape of the Pressure Profile is in Agreement with Some Variation in the Magnitude

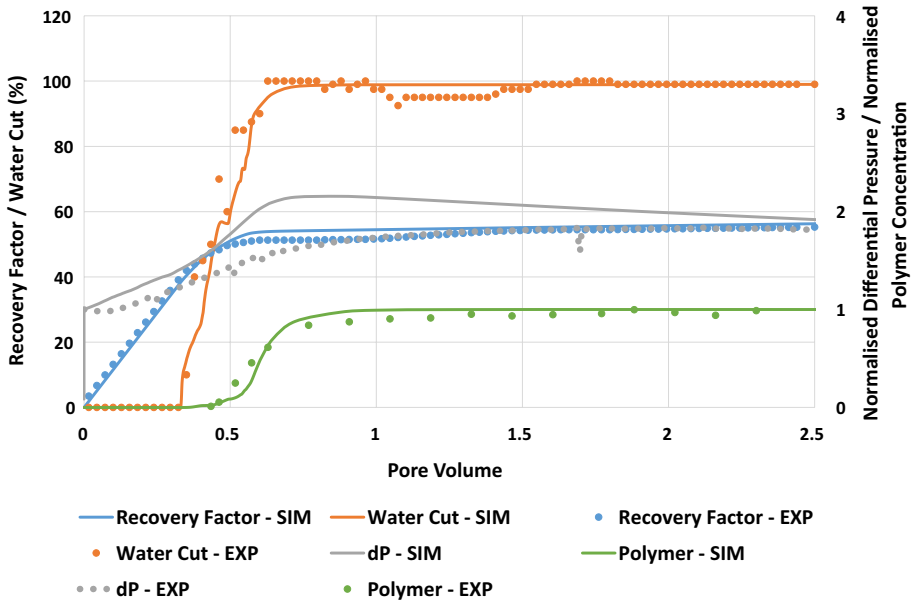


Fig. 7 Secondary Polymer Flood for CF1—Experiment versus Simulation Match. Oil, Water, Pressure and Polymer Concentration are in Good Agreement between Experiment and Simulation

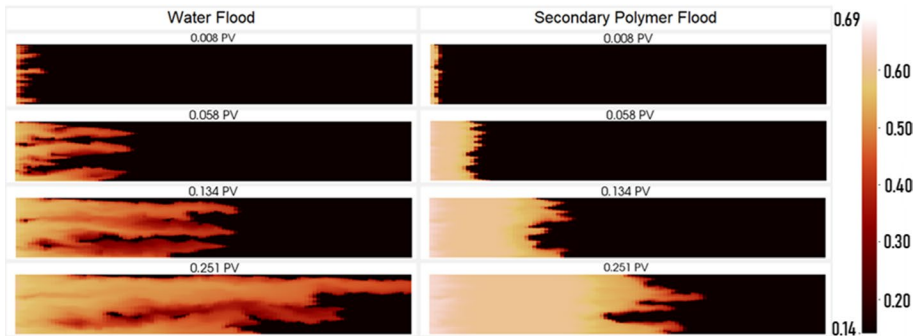


Fig. 8 Waterflood versus Secondary Polymer Flood for CF1—Visualisation of Water Saturation at Specified Pore Volume Throughput. The Formation of Immiscible Fingers is observed in both Cases, although to a Lesser Degree in the Secondary Polymer Flood

3.3 Tertiary Polymer Core Flood

Following the waterflood baseline and reconditioning back to S_{wi} in the CF2 flooding cycle, a tertiary polymer flood was performed. Water was first injected (from S_{wi}) at ~ 3 m/day for 0.5 PV before switching to a 1800 mg/L polymer solution at the same rate. A comparison of the tertiary flood versus the base case waterflood for CF2 is shown in Fig. 10.

Excellent early time (up to 0.5 PV) agreement is found between the two recovery fluids, deviating only when polymer is injected at 0.5 PV. Despite the high water cut ($\sim 80\%$), the

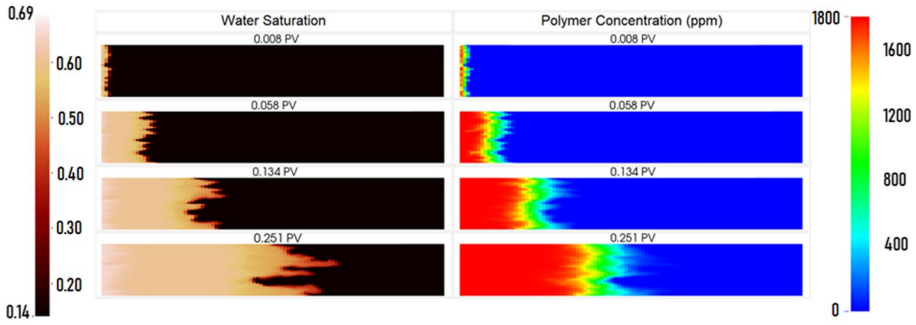


Fig. 9 Secondary Polymer Flood for CF1—Visualisation of Water Saturation vs. Water Phase Viscosity at Specified Pore Volume Throughput. The Polymer Concentration Lags Significantly Behind the Water Fingers Confirming that they are the Result of Banked Connate Water

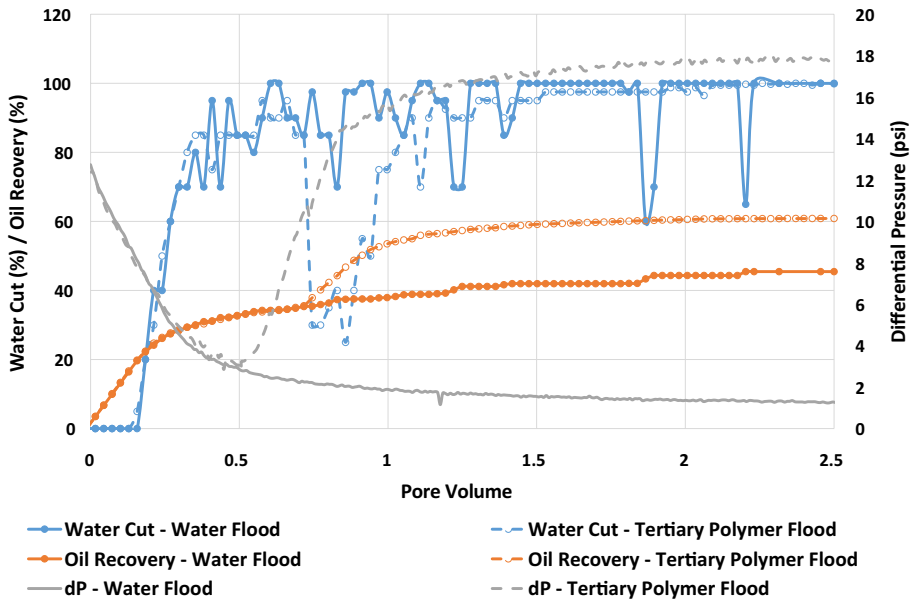


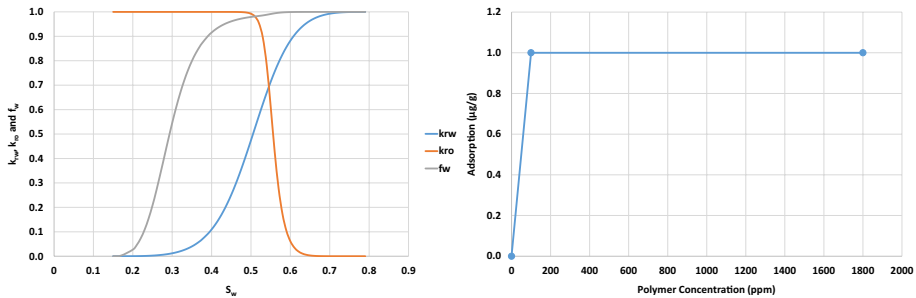
Fig. 10 Tertiary Polymer Flooding vs Waterflooding for CF2 Flooding Cycle. Polymer Flooding in Tertiary Mode at High Water Cut is still able to Significantly Improve Oil Recovery and Decrease Water Cut vs. the WaterFlood

tertiary polymer results in a rapid response in oil production. After 0.25 PV of polymer injection, there is a sharp increase in oil and, correspondingly, a decrease in water cut. At 1 PV total injection, tertiary polymer flooding has increased recovery by 15.6% OOIP, increasing to 17.2% OOIP at 1.5 PV and decreasing slightly to 15.4% OOIP at 2.5 PV. As noted previously, this is very much in line with the proposed viscous crossflow mechanism which is operating in these displacements (Sorbie and Skauge 2019).

Again, referring to the discussion of the M-paradox, we note that using conventional relative permeabilities and a correspondingly low water saturation in the water fingers, it

Table 9 Tertiary polymer flood relative permeability coefficients, adsorption and RRF

α_w	1.0	β_w	2.0	γ_w	3.3	δ_w	1.0	Γ	1 $\mu\text{g/g}$
α_o	1.0	β_o	1.0×10^{-3}	γ_o	15.0	δ_o	2.0	RRF	5.5

**Fig. 11** Tertiary Polymer Flood Relative Permeability, Fractional Flow (left) and Adsorption Isotherm (right)

is not possible to match the large response to the polymer injection. As the methodology used here can both match and predict the response to polymer flooding, immiscible fingers must be present and then the polymer recovery mechanism can be understood as viscous crossflow.

As with the previous polymer flood, minimal polymer retention was measured in the core. At this point, the mobile polymer was flushed from the core with brine at 3 m/day. When the polymer concentration was measured at <0.5 mg/L (>50 PV brine injection), the permeability to water was measured and the RRF determined as at ~ 4.4 . Again, the true RRF may be even higher as the RRF is calculated from the post waterflood permeability at a lower water saturation.

As with the secondary polymer flooding case, experimentation with the relative permeability functions and corresponding fractional flow curve showed an excellent match to the experimental data. The input parameters are given in Table 9, and the various function are shown in Fig. 11.

The match between the experimental and simulated results for the baseline waterflood and the tertiary polymer flood for flooding cycle CF2 are given in Figs. 12 and 13, respectively.

Again, it can be seen for CF2 that there is excellent agreement between simulation and experiment for both baseline waterflood and the tertiary polymer flood. As above, after the flow function adjustment to match the baseline waterflood, no further adjustments were made and hence the polymer simulation is a true *prediction* of the polymer oil recovery mechanism. We note in particular that the polymer simulation gives an almost immediate and accurately reproduced response on the pressure behaviour, the increase in oil recovery and also the drop and subsequent rise in the water cut. The polymer propagation is also accurately matched.

The numerical visualisation of the fingering patterns for the baseline waterflood and the corresponding tertiary polymer flood for the CF2 flooding cycle is shown in Fig. 14. The formation of distinct viscous fingers during the initial 0.5 PV of waterflooding is evident

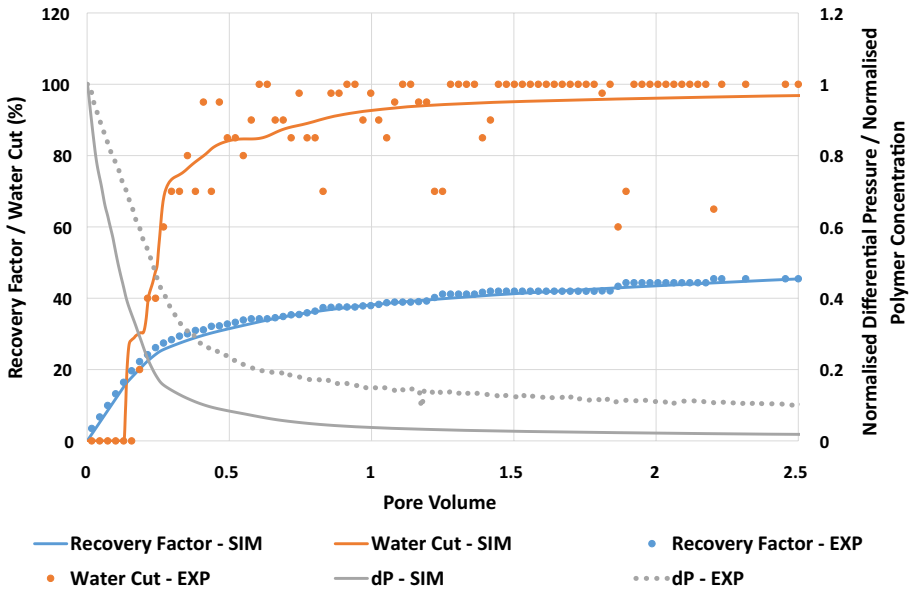


Fig. 12 Tertiary Polymer Flood—Waterflood Baseline in CF2—Experiment versus Simulation Match. Oil and Water Production is Well Matched. The Shape of the Pressure Profile is in Agreement with Some Variation in the Magnitude

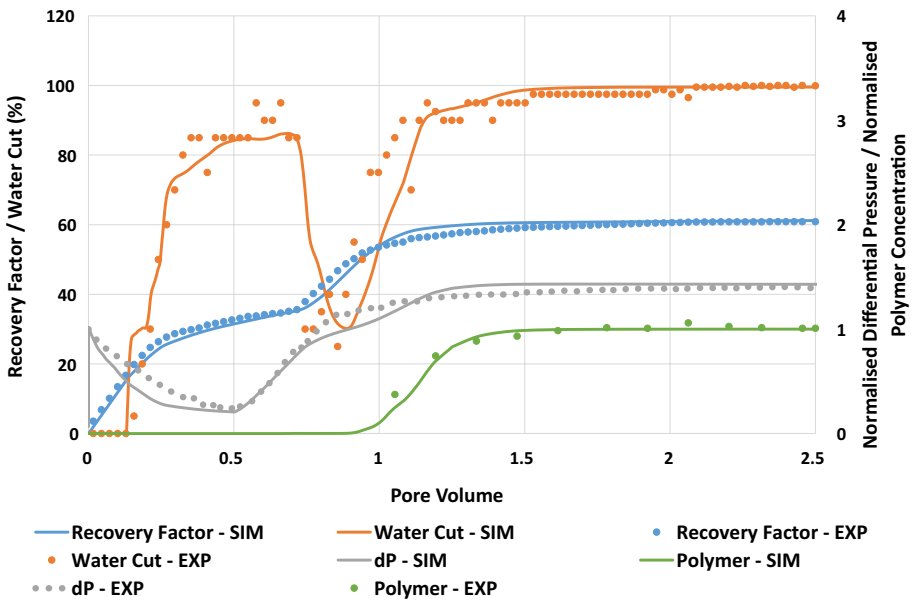


Fig. 13 Tertiary Polymer Flood—Experimental versus Simulation Match for CF2. Oil, Water, Pressure and Polymer Concentration are in Good Agreement between Experiment and Simulation

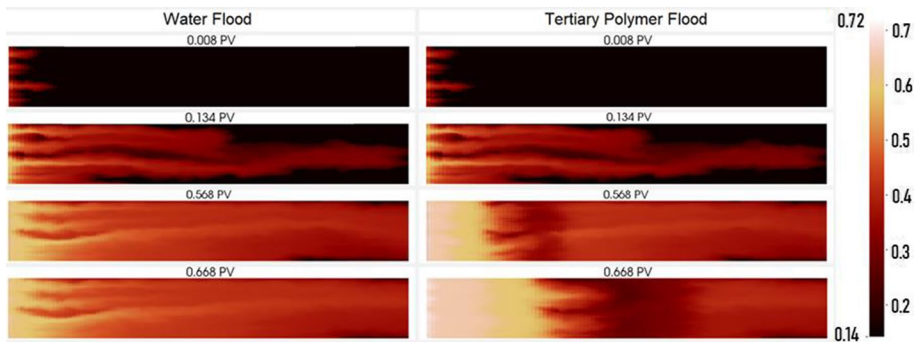


Fig. 14 Waterflood vs Tertiary Polymer Flood for CF2—Visualisation of Water Saturation at Specified Pore Volume Throughput. Prior to 0.5 PV both Cases Show Highly Fingered Systems, the application of Tertiary Polymer Flooding at 0.5 PV Quickly Generates a Strong Oil Bank

in these figures; this leads to the early breakthrough at ~ 0.2 PV and rapid rise in water cut to ~ 80 – 90% .

From the visualisation of the floods, it is evident that a strong oil bank (Fig. 14; tertiary polymer flood at 0.668 PV, bottom right) is formed on injection of polymer. It is this strong oil bank that is responsible for the large and very rapid response of the tertiary polymer flood—directly in line with the experimental observations and the mechanism of viscous crossflow.

3.4 Reducing the Tertiary Polymer Viscosity

From the very good agreement between the simulation and the observations for the tertiary polymer flood, it was possible to predict the answer to certain question using our numerical model. The question which we addressed was as follows: *Is the polymer viscosity optimal, or would a lower polymer viscosity give us an almost equally good response?* Indeed, the authors *did* actually do this calculation as prediction *before* carrying out the experiment. With all other parameters kept constant, the simulated polymer viscosity was reduced to 11 mPa.s and 5 mPa.s. The resulting predicted recovery, water cut and pressure profiles are shown for these assumed lower polymer viscosity values in Fig. 15.

From the predicted response, it is clear that the current system ($\mu_p = 22$ mPa.s) is predicted to be strongly viscous over-stable and thus a significant reduction of the polymer concentration should be possible with minimal decrease in flood performance. In order to test this prediction, a further tertiary polymer core flood cycle (CF3) was performed, with the only variable being the reduced injected concentration ($C = 1260$ mg/L), and this polymer solution has a Newtonian plateau viscosity, $\mu_p = 11$ mPa.s.

As with the previous tertiary polymer flood, water was injected at ~ 3 m/day for 0.5 PV before switching to the polymer solution at the same rate, in flood CF3. A comparison of the reduced viscosity tertiary flood versus the base case waterflood for CF3 is shown in Fig. 16.

Despite the reduced viscosity and adverse water cut ($\sim 80\%$) in CF3, there is a quick and strong response in oil production after ~ 0.25 PV of polymer injection with a corresponding drop in water cut to $\sim 35\%$. The results in Fig. 16 are in excellent agreement with our prediction, shown in Fig. 15. This both confirms the predictive power of our simulation approach. In

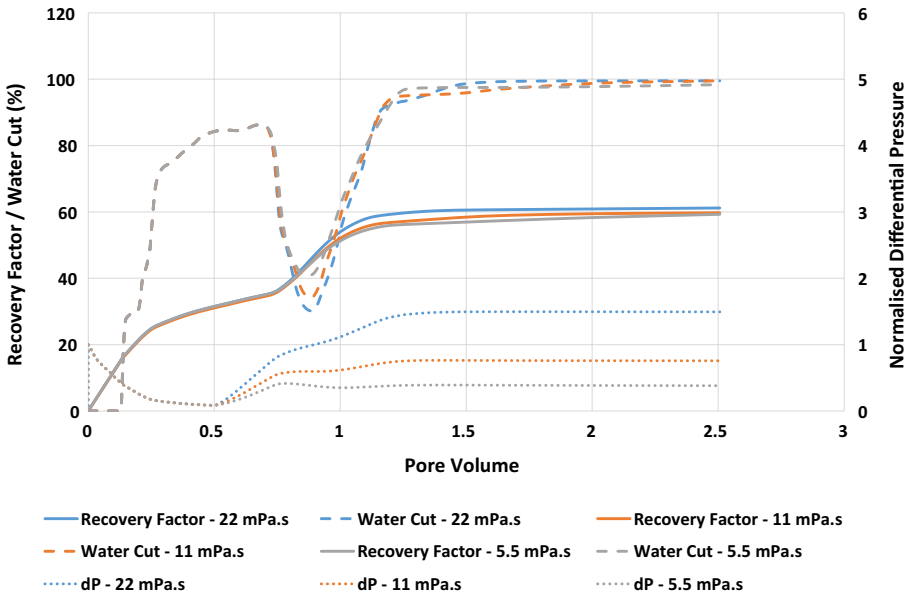


Fig. 15 Simulated Response to Tertiary Polymer Viscosity. The Simulated System is Highly Insensitive to Injection Viscosity down to 5.5 mPa.s

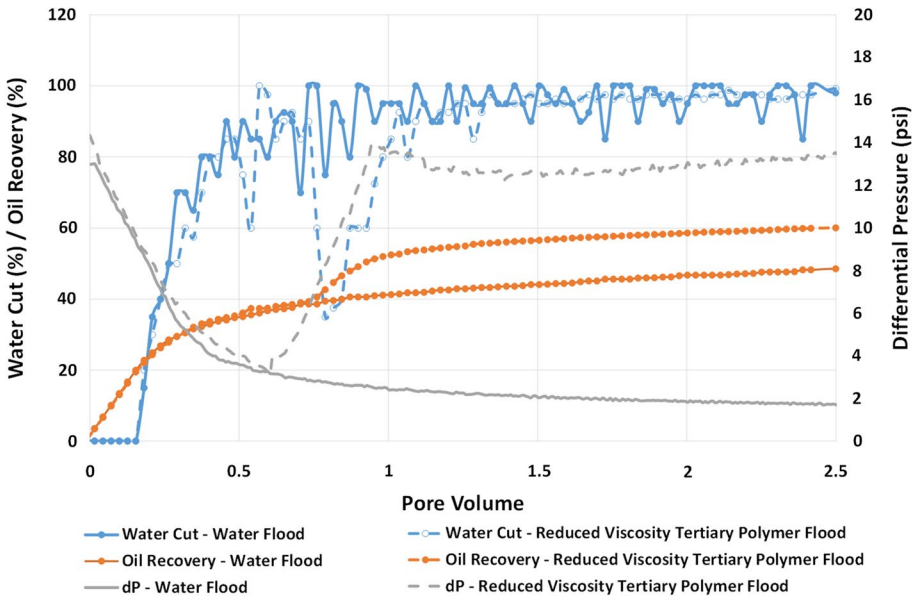


Fig. 16 Reduced Viscosity Tertiary Polymer Flooding vs Waterflooding for CF3 Flooding Cycle. A Reduced Viscosity Polymer Flood Still Shows a High Recovery and Large Decrease in Water Production

Table 10 Reduced viscosity tertiary polymer flood relative permeability coefficients, adsorption and RRF

α_w	1.0	β_w	17	γ_w	4.0	δ_w	1.5	Γ	1 $\mu\text{g/g}$
α_o	1.0	β_o	1.0×10^{-3}	γ_o	15.0	δ_o	2.0	RRF	5.5

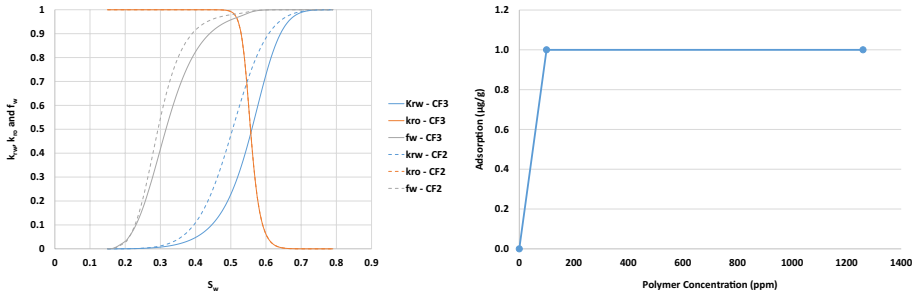


Fig. 17 Tertiary Polymer Flood Relative Permeability, Fractional Flow (left) and Adsorption Isotherm (right). CF2—Tertiary Polymer Flood, CF3—Reduced Viscosity Tertiary Polymer Flood

addition, it also demonstrates that the proposed viscous crossflow mechanism requires only a modest polymer viscosity in order to achieve significant improvements to recovery. At 1 PV total injection, the reduced viscosity tertiary polymer flood has increased recovery by 11.2% OOIP, increasing to 12.5% OOIP at 1.5 PV and decreasing slightly to 11.5% OOIP at 2.5 PV.

Following the same approach as for the previous floods, retention was determined as $< 10 \mu\text{g/g}$ and RRF as > 3.2 .

During the simulation of the reduced viscosity tertiary polymer flood in the CF3 flooding cycle, minor modifications were made to the water relative permeability in order to compensate for the variance in waterflood performance between the two tertiary polymer floods. The revised input parameters are given in Table 10, and the functions are shown in Fig. 17.

The match obtained with the refined water relative permeability curve for the base-line waterflood and reduced viscosity tertiary polymer flood in the CF3 flooding cycle are shown in Figs. 18 and 19, respectively.

With only minor modification to the water relative permeability curve, to account for core-to-core variation, an excellent match to the experimental results is obtained for both water and tertiary polymer flooding. Thus, the methodology presented by Sorbie et al. (2020) is shown to be able to match experimental results, but also to accurately predict both (a) the impact of viscous polymer ($\mu_p = 22 \text{ mPa.s}$) on the system and (b) the relative insensitivity of the reduced viscosity polymer ($\mu_p = 11 \text{ mPa.s}$) viscosity.

4 Impact of Grid Refinement

To confirm the robustness of the simulation methodology and results, repeat simulations of the 22 mPa.s tertiary polymer flood (CF2) were performed using (i) multiple (3) permeability fields generated randomly, but which are statistically identical in terms of heterogeneity and correlation structure, and (ii) at 2 levels of grid refinement.

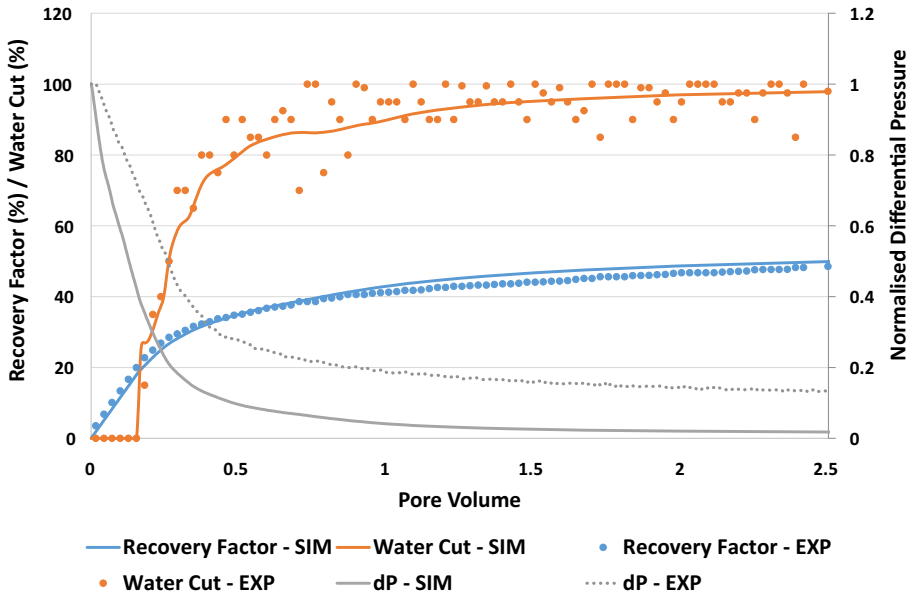


Fig. 18 Reduced Viscosity Tertiary Polymer Flood—Waterflood Baseline for CF3—Experiment versus Simulation Match. Oil and Water Production is Well Matched. The Shape of the Pressure Profile is in Agreement with Some Variation in the Magnitude

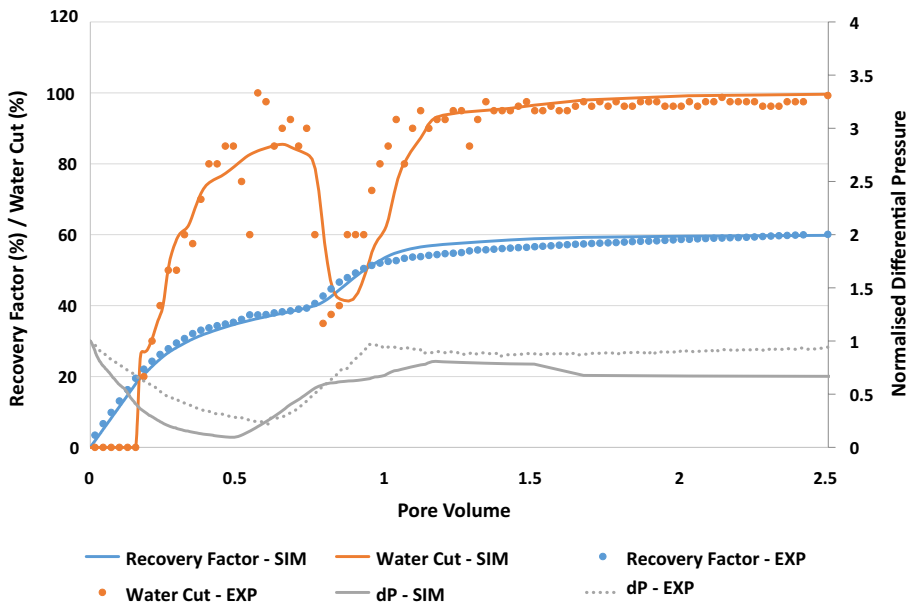


Fig. 19 Reduced Viscosity Tertiary Polymer Flood—Experiment versus Simulation Match for flooding cycle CF3. Oil, Water, Pressure and Polymer Concentration are in Good Agreement between Experiment and Simulation

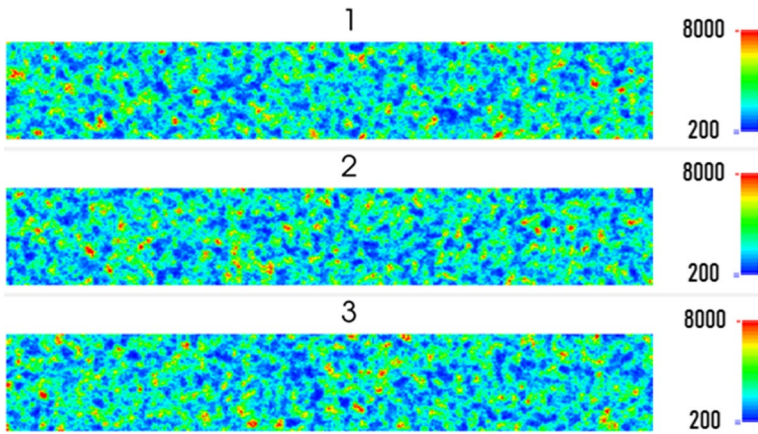


Fig. 20 Permeability Field Iterations 1–3 in 350×350 Grids

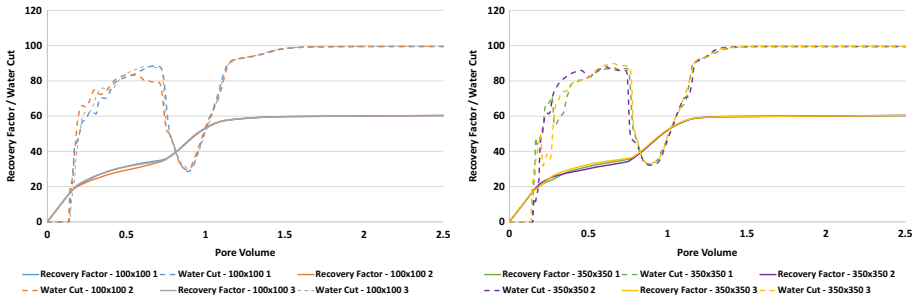


Fig. 21 Impact of Permeability Field Iteration— 100×100 Grid (left) & 350×350 Grid (right). Each Iteration Shows Minimal Variance at a Given Grid Resolution

Three permeability fields were generated using a 500×500 grid—using the same average permeability, correlation length and Dykstra–Parsons coefficient—before coarsening directly to 350×350 or 100×100 grids. The resulting permeability fields are shown in Fig. 20 for the 350×350 grids.

It can be observed that the pattern in each grid varies, but the overall field remains similar between each of the statistical realisations. With the grids in place, the tertiary polymer flood simulation was re-run in each grid realisation at both levels of grid refinement, and results are shown in Fig. 21.

Within a level of grid refinement (e.g. 100×100), there is a minimal sensitivity to the realisation of the permeability field. This is clearly demonstrated by the closeness of the simulated results in Fig. 21. When examining the same permeability field realisation at a different levels of grid refinement a small, but slightly bigger, sensitivity was observed as shown in Fig. 22.

From Fig. 22, it is evident that the level of grid refinement has a small but just visible impact on the production of oil and water. By refining the grid the fingers have been sharpened and the level of numerical dispersion is somewhat reduced. These small changes are a little more evident in the viscous finger patterns shown in Fig. 23. It should be noted that this

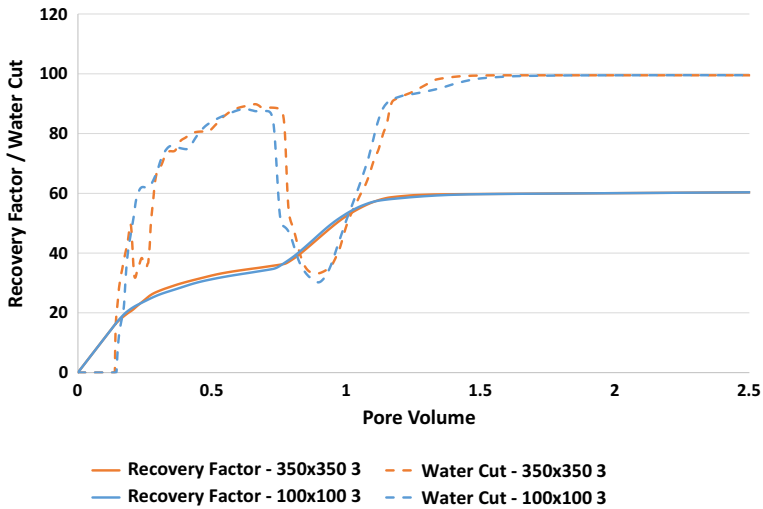


Fig. 22 Impact of Grid Refinement on a Given Permeability Field Iteration—Iteration 3. Only Minor Variation Results from Grid Coarsening from 350×350 to 100×100

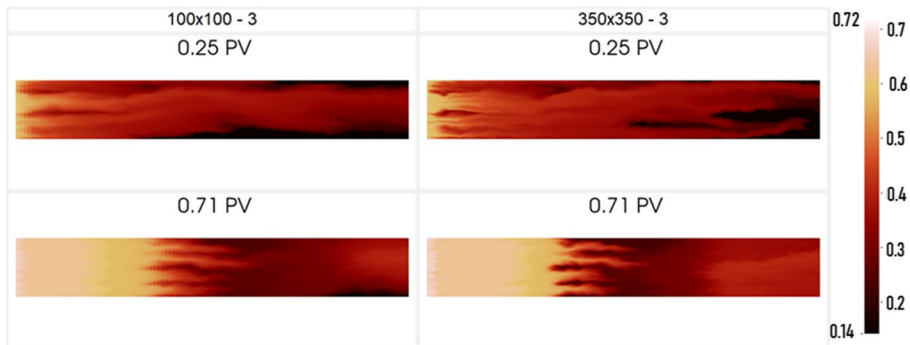


Fig. 23 Impact of Grid Refinement on a Given Permeability Field Iteration—Iteration 3—Water Saturation. Refinement has resulted in Sharpened Fingers and Some Variation to the Pathways due to the Reduced Numerical Dispersion

behaviour is observed for all three realisations of the permeability field; however, the results from realisation 3 have been presented here since this example shows the highest sensitivity to refinement. Indeed, the impact of the actual permeability realisation and level of grid refinement in all cases was minimal. In addition, we found that all results can be brought into line with experimental results by making very minor changes to the relative permeability curves/ fractional flow.

5 Discussion and Comparison of Results

To make an accurate assessment of the recovery from each of the polymer floods under secondary and tertiary conditions, a baseline was established in each core flooding cycle for the corresponding waterfloods. Excellent agreement was observed between the 3 baseline waterfloods (in CF1, CF2 and CF3) and the minor differences seen between them are entirely within acceptable core-to-core variation. Thus, a comparison can be made both between waterflooding and polymer flooding, as well as between the secondary and tertiary modes of recovery and the impact of polymer viscosity on tertiary flooding for oils of moderate viscosity ($\mu_o = 84$ mPa.s, in this case).

A full comparison of the various responses (oil recovery, water cut and pressures) in the waterfloods and the $\mu_p = 22$ mPa.s secondary and tertiary polymer floods is made in Fig. 24.

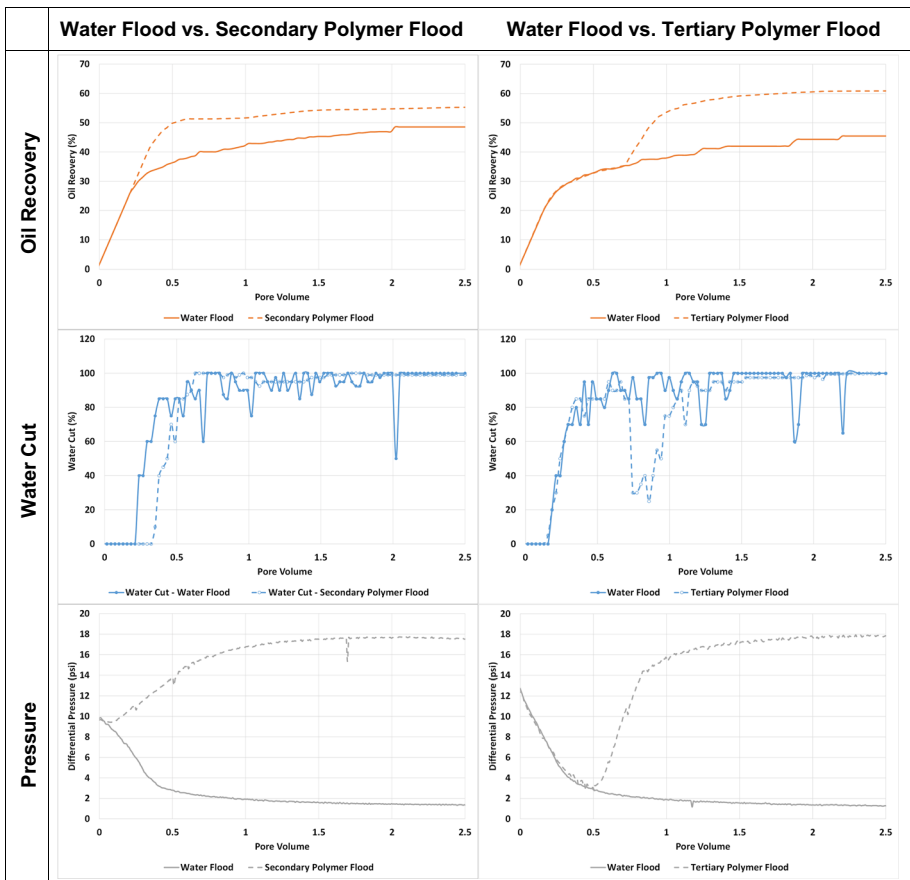


Fig. 24 Secondary Polymer Flooding vs Tertiary Polymer Flooding (with $\mu_p = 22$ mPa.s) versus Water-Flooding. Significant Improvements in Recovery are observed for both Secondary and Tertiary Polymer Flooding vs. WaterFlooding. Delaying the Injection of Polymer to 0.5 PV (i.e. moving from Secondary to Tertiary) does not Result in a loss of Performance

When considering the three recovery modes (water, secondary polymer and tertiary polymer), it is clear than polymer flooding shows excellent incremental recovery potential in this moderately viscous, homogeneous system. The data presented in Fig. 24 clearly illustrate the properties of secondary vs. tertiary polymer flooding. Polymer application in secondary mode considerably delays the water breakthrough compared with the waterflood and brings oil production significantly forward in time. In tertiary mode, despite significant water fingering and high water cut (~80%) after 0.5 PV of water injection, the polymer is able to rapidly mobilise and crossflow the oil and form an oil bank, giving a fast and strong improvement in recovery. This is clear evidence of the recovery mechanism at work, where the injection of the polymer into the established channels causes viscous crossflow of the oil into the faster flowing water fingers from where it is rapidly “banked” and then produced.

In these particular experiments, we observe that the tertiary polymer flood actually outperformed secondary polymer flooding by ~5% OOIP. However, we do *not* conclude in general that tertiary will outperform secondary polymer. This could simply be due to

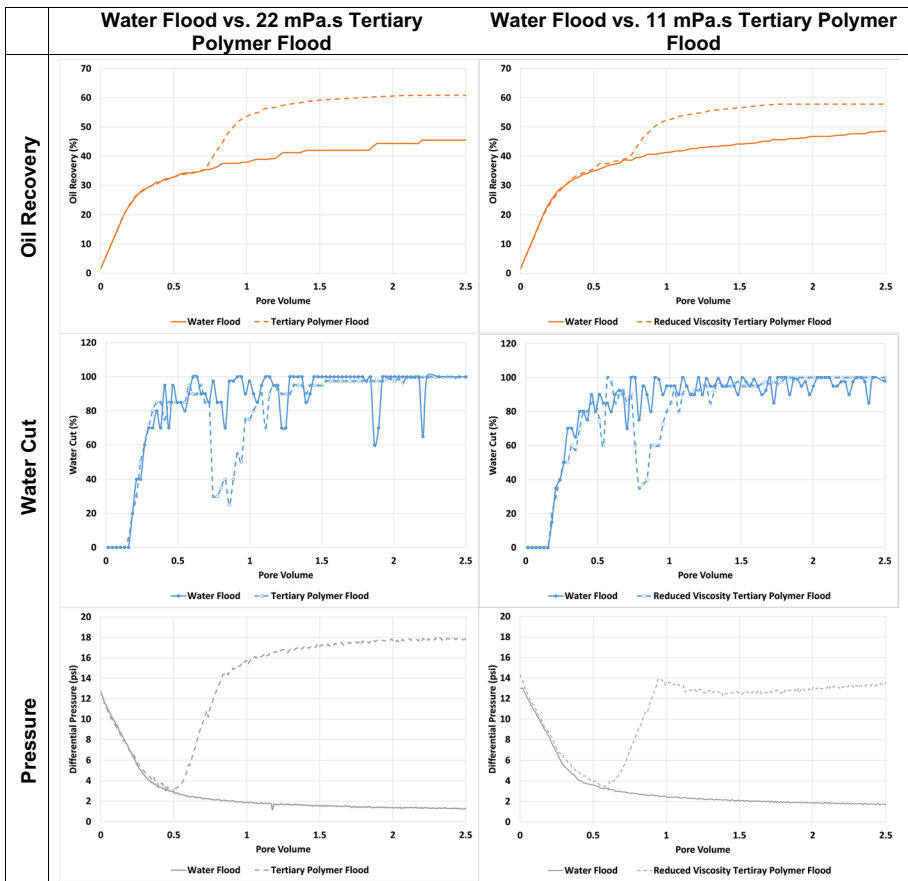


Fig. 25 22 mPa.s versus 11 mPa.s Tertiary Polymer Flooding comparison. Reducing the Injection Viscosity from 22.2 mPa.s to 11 mPa.s has only a Minor Impact on Recovery, while Significantly Reducing the Differential Pressure across the Core

core-to-core variation. However, neither do we conclude that the tertiary oil recovery is significantly *worse* than the secondary polymer flood, as may be expected.

A similar analysis of the impact of reduced viscosity ($\mu_p = 11$ mPa.s) on the performance of tertiary polymer flooding can also be performed, as shown in Fig. 25.

When comparing the performance of 22 and 11 mPa.s, it is immediately apparent that there is not the significant decrease in oil recovery that might be expected. Rather, both floods show a rapid response to polymer injection at 0.5 PV, resulting in an increase in recovery at 1 PV of 15.6% OOIP for the 22 mPa.s slug and 11.2% OOIP for the 11 mPa.s slug over the respective waterflood. This improvement in recovery is continued after 2.5 PV with an additional 15.4% OOIP for the 22 mPa.s slug and 11.5% OOIP for the 11 mPa.s slug over the respective waterflood. By reducing the viscosity of the injected slug by 50%, it has been possible to achieve > 70% of the recovery of the initial polymer slug design with a significant reduction in injection pressure.

These results show good agreement with those presented by Seright et al. (2018), Skauge et al. (2012), and Skauge et al. (2014), clearly demonstrating that the proposed viscous crossflow mechanism (Sorbie and Skauge 2019) continues to apply at moderate oil viscosities and in relatively homogeneous systems. Furthermore, the methodology developed by Sorbie et al. (2020) has been validated for such systems and has been shown to be capable of achieving excellent agreement with experimental results for systems showing immiscible viscous fingering, which is then subsequently modified by the injection of tertiary polymer.

6 Summary and Conclusions

A series of core flooding experiments has been carried out to examine the impact of polymer flooding (secondary and tertiary) on the recovery of a moderately viscous crude oil ($\mu_o = 84$ mPa.s). It has been shown that the application of polymer can be assessed directly in core plugs and shows a significant improvement in recovery regardless of the mode of injection, secondary or tertiary. Furthermore, the methodology proposed by Sorbie et al. (2020) has enabled very close matching of simulation to the experimental observations. Such a match is only possible if the viscous fingering processes are correctly modelled in the core. With simple adjustment to the simulation grid properties, relative permeabilities and the fractional flow curve, the presence of viscous fingering in these core flood experiments is well captured by our approach. Furthermore, this approach uses standard reservoir simulators employing elementary numerical methods (single-point upstreaming).

In the case of the tertiary polymer flood, the core was first flooded with 0.5 PV of water at 3 m/day (80% water cut), before switching to injecting polymer ($C = 1800$ mg/L, $\mu_p = 22$ mPa.s) at the same injection rate for 2.0 PV. This polymer application, even though it was applied at a high water cut, showed a strong impact on recovery, bringing the oil recovery significantly forward in time, and immediately dropping the water cut from 80 to ~30%. By 1.5 PV of total injection, tertiary polymer flooding showed an incremental recovery of 40% over waterflooding at that time.

A predictive simulation based on the 22 mPa.s polymer flood case suggested that only a minimal loss of recovery would be observed by reducing the viscosity by half. This led us to perform a second tertiary lower viscosity polymer flood ($C = 1260$ mg/L, $\mu_p = 11$ mPa.s) to validate this prediction. The reduced viscosity flood was able to achieve 70% of the

incremental recovery of the 22 mPa.s flood at 1 PV and at 2.5 PV total injection, while showing a significant decrease in injection pressure.

During the secondary polymer flood, the core was injected with polymer from the start of the two-phase flood, where $S_w = S_{wi}$. As with the tertiary polymer flood, the oil recovery was brought forward in time; however, the incremental recovery over the corresponding waterflood was somewhat lower. By 1.5 PV of injection, secondary polymer flooding showed an incremental recovery of 20% over waterflooding at the same stage. We note that *viscous fingering is still predicted for the secondary polymer flood* since the in situ (connate) water is still of low viscosity ($\mu_w \sim 0.81$ mPa.s), and this connate water is banked and the front is then unstable. The polymer does suppress this fingering to some degree, but it does not eliminate it (see Fig. 8).

This observed behaviour during these floods is in line with the viscous fingering and viscous crossflow mechanisms described in the literature (Sorbie et al. 2020; Sorbie and Skauge 2019). This demonstrates the significant potential of polymer flooding as a tertiary recovery mechanism in homogeneous systems with moderate/high oil viscosity, even at relatively low polymer dosages.

The observations clearly point to the occurrence of immiscible viscous fingering in the waterflood, even at the core scale. As the size scale increases, then these small fingers will be “washed out”, but they will be replaced by dominant fingers at a larger scale determined by the effective dispersivity (mixing) in the reservoir. When polymer is applied, contrary to conventional wisdom, this does not stop the fingering and completely stabilise the front. The polymer also shows some degree of fingering along the dominant water fingers, but these more viscous “tendrils” of polymer flow lead to viscous crossflow of bypassed oil into the main flow channels from whence the oil is visibly banked and then produced. This overall viscous crossflow mechanism in tertiary polymer mode is described in detail in Sorbie et al (2020), and it is characterised by a very quick (after ~ 0.2 PV) and large ($> 40\%$) response in incremental oil recovery.

This experimental study has been carried out in support of an actual field polymer flood in Field X. A companion paper to this work is currently in preparation, taking the experimental results and simulation matches obtained here and “upscaling” them to reservoir scale models to better understand the impact of immiscible viscous fingering and subsequent polymer injection on field scale polymer flooding operations.

Acknowledgements The authors thank the associate editor and anonymous reviewers from Transport in Porous Media. Their insightful comments and suggestions were greatly appreciated.

Declarations

Conflict of interest Not applicable.

Open Access This article is licensed under a Creative Commons Attribution 4.0 International License, which permits use, sharing, adaptation, distribution and reproduction in any medium or format, as long as you give appropriate credit to the original author(s) and the source, provide a link to the Creative Commons licence, and indicate if changes were made. The images or other third party material in this article are included in the article’s Creative Commons licence, unless indicated otherwise in a credit line to the material. If material is not included in the article’s Creative Commons licence and your intended use is not permitted by statutory regulation or exceeds the permitted use, you will need to obtain permission directly from the copyright holder. To view a copy of this licence, visit <http://creativecommons.org/licenses/by/4.0/>.



References

- Berg, S., Ott, H.: Stability of CO₂-brine immiscible displacement. *Int. J. Greenhouse Gas Control* **11**, 188–203 (2012). <https://doi.org/10.1016/j.ijggc.2012.07.001>
- Beteta, A., Nurmi, L., Rosati, L., Hanski, S., McIver, K., Sorbie, K., Toivonen, S.: Impact of Acrylate and 2-Acrylamido-Tertiary-Butyl Sulfonic acid content on the enhanced oil recovery performance of synthetic polymers. *SPE J.* **26**(04), 2092–2113 (2021). <https://doi.org/10.2118/200441-PA>
- Buckley, S.E., Leverett, M.C.: Mechanism of fluid displacement in sands. *Trans. AIME* **146**(01), 107–116 (1942). <https://doi.org/10.2118/942107-G>
- Christie, M.A.: High-resolution simulation of unstable flows in porous media. *SPE Reser. Eng.* **4**(3), 297–303 (1989). <https://doi.org/10.2118/16005-pa>
- Clemens, T., Tskouris, K., Buchgraber, M., Castanier, L., Kovscek, A.: Pore-scale evaluation of polymers displacing viscous oil-computational- fluid-dynamics simulation of micromodel experiments. *SPE Reser. Eval. Eng.* **16**(2), 144–154 (2013). <https://doi.org/10.2118/154169-PA>
- Daripa, P., Glimm, J., Lindquist, B., McBryan, O.: Polymer floods: a case study of nonlinear wave analysis and of instability control in tertiary oil recovery. *SIAM J. Appl. Math.* **48**(2), 353–373 (1988). <https://doi.org/10.2307/2101612>
- Delamaide, E., Zaitoun, A., Renard, G., Tabary, R.: Pelican lake field: first successful application of polymer flooding in a heavy oil reservoir. *SPE Reser. Eval. Eng.* **17**(03), 2–4 (2014). <https://doi.org/10.2118/165234-PA>
- Dong, B., Yan, Y.Y., Li, W.Z.: LBM simulation of viscous fingering phenomenon in immiscible displacement of two fluids in porous media. *Transp. Porous Media* **88**, 293–314 (2011). <https://doi.org/10.1007/s11242-011-9740-y>
- Dykstra, H., Parsons, R.L.: The prediction of oil recovery by waterflood (2nd Editio). Dallas: American Petroleum Institute. (1950)
- Engelberts, W.F., Klinkenberg, L.J.: Laboratory experiments on the displacement of oil by water from packs of granular material. Presented at the 3rd World Petroleum Congress, The Hague, the Netherlands, 28 May–6 June. WPC-4138. (1951)
- Homsy, G.M.: Viscous fingering in porous media. *Ann. Rev. Fluid Mech.* **19**(1), 271–311 (1987). <https://doi.org/10.1146/annurev.fl.19.010187.001415>
- Jerauld, G.R., Davis, H.T., Scriven, L.E.: Stability fronts of permanent form in immiscible displacement. Presented at the SPE annual technical conference and exhibition, Houston, Texas, 16–19 September. SPE-13164. (1984) <https://doi.org/10.2118/13164-MS>
- Johnson, E.F., Bossler, D.P., Bossler, V.O.N.: Calculation of relative permeability from displacement experiments. *Trans. AIME* **216**(01), 370–372 (1959). <https://doi.org/10.2118/1023-g>
- Juanes, R., Blunt, M.J.: Analytical solutions to multiphase first-contact miscible models with viscous fingering. *Transp. Porous Media* **64**(3), 339–373 (2006). <https://doi.org/10.1007/s11242-005-5049-z>
- Lenormand, R., Touboul, E., Zarcone, C.: Numerical models and experiments on immiscible displacements in porous media. *J. Fluid Mech.* **189**, 165–187 (1988). <https://doi.org/10.1017/S0022112088000953>
- Luo, H., Delshad, M., Zhao, B., Mohanty, K.K.: A Fractional flow theory for unstable immiscible floods. Presented at the SPE Canada heavy oil technical conference, Calgary, Alberta, Canada, 15–16 February. SPE-184996. (2017) <https://doi.org/10.2118/184996-ms>
- McPhee, C., Reed, J., Zubizarreta, I.: Core analysis: a best practice guide. Elsevier, Amsterdam (2015)
- Pereira, B., Shahverdi, H., Sohrabi, M.: Refinement of relative permeability measurements by accounting for viscous fingering in coreflood experiments. Presented at the SPE annual technical conference and exhibition, Amsterdam, The Netherlands, 27–29 October. SPE170717. (2014) <https://doi.org/10.2118/170717-ms>
- Pinilla, A., Asuaje, M., Ratkovich, N.: Experimental and computational advances on the study of viscous fingering: an umbrella review. *Heliyon* (2021). <https://doi.org/10.1016/j.heliyon.2021.e07614>
- Pye, D.J.: Improved secondary recovery by control of water mobility. *J. of Petrol. Technol.* **16**(08), 911–916 (1964). <https://doi.org/10.2118/845-pa>
- Regaieg, M., McDougall, S.R., Bondino, I., Hamon, G.: Finger thickening during extra-heavy oil waterflooding: simulation and interpretation using pore-scale modelling. *PLoS ONE* **12**(1), 1–28 (2017). <https://doi.org/10.1371/journal.pone.0169727>
- Salmo, I.C., Sorbie, K.S., Skauge, A., Alzaabi, M.A.: Immiscible viscous fingering : modelling unstable water-oil displacement experiments in porous media. Submitted for Publication. (2022)
- Sandiford, B.B.: Laboratory and field studies of waterfloods using polymer solutions to increase oil recoveries. *J. Petrol. Technol.* **16**(08), 917–922 (1964). <https://doi.org/10.2118/844-PA>

- Seright, R.S., Wang, D., Lerner, N., Nguyen, A., Sabid, J., Tochor, R.: Can 25-cP polymer solution efficiently displace 1,600-cP oil during polymer flooding? *SPE J.* **23**(6), 2260–2278 (2018). <https://doi.org/10.2118/190321-PA>
- Shields, R.A., Sorbie, K.S., Singleton, M.A., Guan, H.: Analysis of the mechanism of transport and retention of nonaqueous scale-inhibitor treatments in cores using novel tracer techniques. Presented at the SPE international oilfield scale symposium, Aberdeen, UK, 31 May–1 June. SPE-100518. (2006) <https://doi.org/10.2118/100518-MS>
- Skauge, A., Ormehaug, P.A., Gurholt, T., Vik, B., Bondino, I., Hamon, G.: 2-D visualisation of unstable waterflood and polymer flood for displacement of heavy Oil. SPE Improved Oil Recovery Conference Tulsa, Oklahoma, USA, 14–18 April. SPE-154292. (2012)<https://doi.org/10.2118/154292-MS>
- Skauge, T., Vik, B.F., Ormehaug, P.A., Jatten, B.K., Kippe, V., Skjevraak, I., Standnes, D.C., Uleberg, K., Skauge, A.: Polymer flood at adverse mobility ratio in 2D Flow by X-ray visualization. Presented at the SPE EOR conference at oil and gas West Asia, Muscat, Oman, 31 March - 2 April. SPE-169740. (2014)<https://doi.org/10.2118/169740-MS>
- Sorbie, K.S.: Polymer improved oil recovery, 1st edn. Blackie, Glasgow (1991)
- Sorbie, K.S., Al Ghafri, A.Y., Skauge, A., Mackay, E.J.: On the modelling of immiscible viscous fingering in two - phase flow in porous media. *Transp. Porous Media* **135**(2), 331–359 (2020). <https://doi.org/10.1007/s11242-020-01479-w>
- Sorbie, K.S., Skauge, A.: Mobilization of by-passed oil by viscous crossflow in EOR processes. Presented at the 20th European symposium on improved oil recovery, Pau, France, 8–11 April. (2019) <https://doi.org/10.3997/2214-4609.201900057>
- Tai, I., Muggeridge, A.: Evaluation of empirical models for viscous fingering in miscible displacement. 20th EAGE European symposium on improved oil recovery, Pau, France, 8–11 April, (2019)<https://doi.org/10.3997/2214-4609.201900138>
- van Meurs, P., van der Poel, C.: A theoretical description of water-drive processes involving viscous fingering. *Petrol. Trans. AIME* **213**(01), 103–112 (1958). <https://doi.org/10.2118/931-g>
- Yortsos, Y.C., Hickernell, F.J.: Linear stability of immiscible displacement in porous media. *SIAM J. Appl. Math.* **49**(3), 730–748 (1989). <https://doi.org/10.1137/0149043>

Publisher's Note Springer Nature remains neutral with regard to jurisdictional claims in published maps and institutional affiliations.

Authors and Affiliations

A. Beteta¹  · K. S. Sorbie¹  · K. McIver¹ · G. Johnson² · R. Gasimov² · W. van Zeil²

✉ A. Beteta
a.beteta@hw.ac.uk

¹ Institute of GeoEnergy Engineering, Heriot-Watt University, Edinburgh, UK

² Ithaca Energy (UK) Limited, Hill of Rubislaw, Aberdeen, UK